Chapter 1
Trimmed Spline Surfaces with Accurate Boundary Control

Florian Martin and Ulrich Reif

Abstract We introduce trimmed NURBS surfaces with accurate boundary control, briefly called ABC-surfaces, as a solution to the notorious problem of constructing watertight or smooth (G^1 and G^2) multi-patch surfaces within the function range of standard CAD/CAM systems and the associated file exchange formats. Our construction is based on the appropriate blend of a base surface, which traces out the intended global shape, and a series of reparametrized ribbons, which dominate the shape near the boundary.

1.1 Introduction

Trimmed NURBS surfaces are the standard for industrial surface modeling, today. This class of surfaces combines computational efficiency, geometric flexibility, and ease of use for the designer. All current CAD/CAM systems and various file exchange formats support this–and typically only this–method. While the advantages of trimmed NURBS are undisputed, there is one severe and persistent shortcoming that has not found a commonly accepted solution in decades: multi-patch arrangements of trimmed NURBS surfaces are typically discontinuous along common boundary curves of neighboring pieces. The problem is the following: Given a tensor product spline surface $\mathbf{s} : \mathbb{R}^2 \to \mathbb{R}^3$, current CAD systems provide two ways of representing the boundaries of a trimmed NURBS surface. Either one can use a planar spline curve $\gamma : \mathbb{R} \to \mathbb{R}^2$ to bound the domain or one can use a spatial spline curve $\mathbf{c} : \mathbb{R} \to \mathbb{R}^3$ to bound the trace. The first variant leads to the boundary curve $\mathbf{s} \circ \gamma$ in three-space. This is a spline curve, again, but typically, it has high degree and many knots, stemming not only from the breaks of γ but also from all points where the trace of γ intersects a knot line of $\mathbf{s}$. The resulting knot structure is uneven and hardly predictable[1]. This fact makes it virtually impossible to match

---

[1] Basically, the only case which does not lead to exploding complexity is the special situation where γ parametrizes a straight line parallel to one of the coordinate axes.

$\mathbf{s} \circ \gamma$ with any other surface boundary at reasonable expense. The second variant is equally discouraging. It seems to be impossible to find a surface $\mathbf{s}$ and a curve $\mathbf{c}$ such that the trace of $\mathbf{s}$ contains the trace of $\mathbf{c}$ exactly. The makeshift for this problem is to accept disjoint traces, and to project $\mathbf{c}$ onto $\mathbf{s}$ in order to determine the actual trimming curve. In general, however, this curve is no longer a spline and again not suitable for a watertight match with a neighboring patch.

To avoid the described problem, one can try to find arrangements of patches for the desired shape which do without trimming. This approach leads to methods like geometric continuity [Pet02], singular parametrization [Rei97], or subdivision [PR08], and also to a variety of constructions for n-sided patches [PGVACN06, VSK16]. As a matter of fact, none of these concepts has found widespread acceptance in industrial CAD/CAM applications. It may be speculated that a certain perseverance of designers and executives is responsible for that situation. However, there is also a more solid explanation. The flow of parametric lines is most important for the design process[2]. On one hand, the parametric lines should follow the shape characteristics (e.g., ridges or curvature lines) of the desired surface to obtain convincing results. On the other hand, a 'natural' arrangement of control meshes greatly favors the intuitive character of interactive modeling techniques. Thus, there is little flexibility in the choice of an adequate parametrization, and the corresponding patches must be trimmed at places where neighbors meet. To sum up, the advantages of a well-adapted parametrization seem to be rated higher than the notorious trouble with the trimming issue.

In CAD/CAM applications, the usual solution to the problem of nonmatching trimming curves is to simply accept little gaps in surface representations, and to make them so small that they do not impair the quality of the product to be manufactured. This allows modeling surfaces of adequate quality, but the price to pay is a certain inconvenience of the design process. The challenge is to design patches that are not only fair by themselves but join with neighbors within a typically very small margin[3]. Further, not only positions must be matched, but possibly also surface normals and curvature tensors in the sense of an approximate G^1- or G^2-continuity of the composite surface. For high quality surface design, as requested for instance in the automotive industry, the only way to achieve this is a time-consuming manual process of iterated boundary adaption and fairing.

Besides these practical considerations, there is another issue with the current state of technology. Surface models with disconnected pieces are not well suited for simulation purposes. No matter how small the gaps are, they appear insurmountable[4] for heat conduction, transmission of forces and bending moments, or other physical processes. For this reason, multi-patch CAD models are usually converted to watertight meshes by elaborate procedures to prepare them for simulation. Volumetric modeling techniques as requested for Isogeometric Analysis with its potential to

---

[2] This observation is a blatant contradiction to the concepts of differentiable geometry, which rely on the *independence* of geometric properties of the chosen parametrization.

[3] Customary tolerances for traditional production techniques have to be decreased even further for modern 3d printing systems with their incredible attention to detail.

[4] Advanced methods like discontinuous Galerkin may offer a remedy.
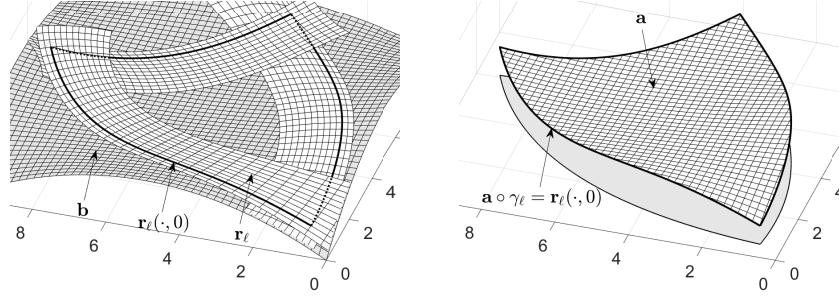
Fig. 1.1 Base **b** and ribbons $\mathbf{r}_\ell$ *(left)*; ABC-surface **a** *(right)*.

save this effort are currently studied. However, they seem to be quite far from a breakthrough for freeform surface design in industrial applications.

From the abundance of material on the design of surfaces of arbitrary topology in general and trimmed NURBS in particular, we want to briefly mention only two recent approaches. In [MH17], a procedure for converting an assembly of trimmed NURBS patches to a watertight model is suggested. It is based on local remodeling such that trimming curves become parametric lines. Without doubt, this is a reasonable practical procedure, even though some issues with a special kind of singularities appearing there (cf. [MR]) and also general fairness aspects are still waiting for a detailed assessment and analysis. Another line of research that has to be discussed in this context is documented in [VSVS20, VVSS20]. It is based on ideas similar those presented here, but there are also significant differences. Before we compare the methods, we briefly explain the basic principles of our approach.

Let **b** be a spline surface, called *base*, and $\mathbf{r}_1, \ldots, \mathbf{r}_L$ be a sequence of other spline surfaces, called *ribbons*. Then we define the *ABC-surface*

$$\mathbf{a} := \frac{w \cdot \mathbf{b} + \sum_{\ell=1}^{L} w_\ell \cdot \mathbf{r}_\ell \circ \kappa_\ell}{w + \sum_{\ell=1}^{L} w_\ell}$$

with suitable reparametrizations κ_ℓ and weight functions w and w_ℓ. Figure 1.1 illustrates the setting. It is instructive, but not necessary, to think of **b** as a standard spline surface describing the overall shape to be designed. When trimmed, its boundaries are close to the desired behavior, but do not match exactly. The ribbons $\mathbf{r}_\ell$ are employed to adjust that deviation.

The domain $\Gamma \subset \mathbb{R}^2$ of **a** is assumed to be bounded by L smooth segments $\Gamma_1, \ldots, \Gamma_L$ meeting at corners $\sigma_1, \ldots, \sigma_L$. The base **b** describes the intended shape globally on Γ, and each ribbon $\mathbf{r}_\ell$ describes that shape locally in a vicinity of the segment Γ_ℓ of the boundary. This is done in such a way that the spline curve $\mathbf{c}_\ell := \mathbf{r}_\ell(\cdot, 0)$ parametrizes the segment $\mathbf{a}(\Gamma_\ell)$ of the boundary of the trace of **a**. The reparametrizations κ_ℓ are used to reconcile the otherwise unrelated surface representations, and the weights are used for blending. When approaching the boundary, w vanishes and makes the base disappear. Further, near the boundary segment $\Gamma_j \subset \mathbb{R}^2$

corresponding to $\mathbf{c}_j$ all weights w_ℓ except for w_j vanish so that also all ribbons but $\mathbf{r}_j$ are faded out. Hence, this surface dominates the behavior of $\mathbf{a}$ near the boundary in a way that will be made precise below. The *accurate boundary control* of the surface $\mathbf{a}$ by means of ribbons explains the acronym *ABC-surface*.

The basic principle and some technical details of ABC-surfaces were first presented in [Rei]. Roughly at the same time and independent of our research, another group developed similar ideas [VVSS20], which were recently brought to our attention. The formal similarities are obvious, but there are also differences, and one of them is significant.

First, the weighted base $w\mathbf{b}$ does not appear in that form[5] in [VVSS20]. Instead, a linear combination $\sum_j b_j \mathbf{p}_j$ of control points $\mathbf{p}_j \in \mathbb{R}^3$ and B-splines b_j is used, where only B-splines with support completely contained in the domain of the surface are permitted so that there is no influence on the shape near the boundary. Accordingly, the term w in the denominator is replaced by $\sum_j b_j$. This can be considered a minor technical detail, but it also reveals a slightly different, though equally valid philosophy behind the construction. We think of the base as a relatively accurate description of the entire surface, and of the ribbons as small, local correctives, used only to adapt $\mathbf{b}$ to the desired boundary behavior. By contrast, the ribbons in [VVSS20] are the major building blocks for the shape to be modeled. The summands $b_j \mathbf{p}_j$, if included at all, are only used for variations inside if the shape defined by the ribbons alone does not yet meet expectations.

Second, and this difference is much more important, the surfaces constructed in [VSVS20, VVSS20] are *transfinite* in the sense that they do not possess a closed-form representation by means of elementary functions. In particular, these surfaces are not piecewise polynomial or rational and thus cannot be stored in standard file formats, as requested in many applications. The point is that the curves γ_ℓ bounding the domain Γ are defined *explicitly* as splines. Once this is done, there is no way to continue the construction within the spline framework. For instance, it is in general impossible to find splines w_ℓ that vanish on all but one of these boundary curves[6]. In [VSVS20, VVSS20], it is suggested to construct reparametrizations and weights as solutions of variational problems with the curves γ_ℓ providing the boundary conditions. This requests a certain computational effort, but visually, the results appear to be excellent. By contrast, in our construction, the boundary curves γ_ℓ are defined *implicitly* as zero levelsets of spline functions. That way, the problem described above disappears. It may be objected that explicit evaluation of the boundary of the domain is now much more expensive than it was before, but as a matter of fact, this is hardly ever requested in practice as long as the spatial boundary curves $\mathbf{c}_\ell$ are available.

The paper is organized as follows: In the next section, we introduce and analyze the basic principle for the construction of ABC-surfaces in a very general setting. Three theorems concerning the behavior of positions, normals, and curvature tensors

---

[5] It does appear in a similar form in [VSR12] for the special case of straight boundaries and polynomial ribbons.

[6] The special case of straight boundaries, which admits rational constructions, was discussed in [VSR12, SVR14, VSK16, VSK17].
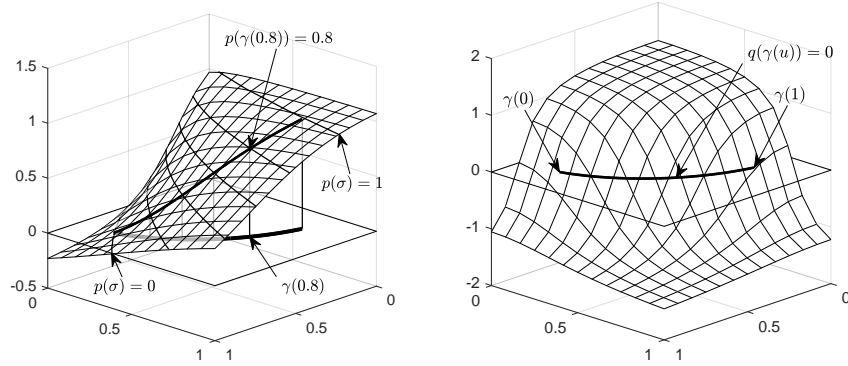
**Fig. 1.2** Parametrizing function *p (left)* and implicit representation *q (right)*.

at the boundary are provided. They establish the validity of our construction, but also that of the methods presented in the more application-oriented papers [SVR14, VSVS20, VVSS20]. In Section 3, we specialize the principle to the spline setting and describe in detail how to construct adequate reparametrizations and weights from given bases and ribbons. Section 4 addresses some important technical issues related to the limitations of current standard formats for file exchange with respect to trimming. Finally, in Section 5, we present a few examples of ABC-spline surfaces to demonstrate the potential of our method.

1.2 Basic principle

Throughout, boldface letters denote points and functions with values in $\mathbb{R}^3$, while greek letters denote points and functions with values in $\mathbb{R}^2$. Except for the surface **a** to be constructed, all functions appearing below are assumed to be sufficiently smooth. In particular, their derivatives mentioned anywhere (explicitly or implicitly through notions like normals or curvatures) are assumed to exist and to be continuous. Further, to avoid a discussion of degenerate cases, surfaces are always assumed to be immersed, i.e., the partial derivatives are linearly independent everywhere. The following definitions are crucial for the construction of ABC-surfaces:

Definition 1 The function $p : \mathbb{R}^2 \to \mathbb{R}$ *parametrizes* the planar curve $\gamma : [0,1] \to \mathbb{R}^2$ if $p(\gamma(u)) = u$ for all $u \in [0,1]$, see Figure 1.2 *(left)*. The function $q : \mathbb{R}^2 \to \mathbb{R}$ is an *implicit representation* of the planar curve γ if $q(\gamma(u)) = 0$ for all $u \in [0,1]$, see Figure 1.2 *(right)*. The function $\kappa := [p,q] : \mathbb{R}^2 \to \mathbb{R}^2$ *defines* γ if there exists a unique regular curve $\gamma : [0,1] \to \mathbb{R}^2$ with implicit representation q that is parametrized by p.

Now, we describe the construction of a surface **a**, whose domain $\Gamma \subset \mathbb{R}^2$ of definition is bounded by a sequence $\gamma_1, \ldots, \gamma_L$ of planar *trimming curves* $\gamma_\ell : [0,1] \to \mathbb{R}^2$.
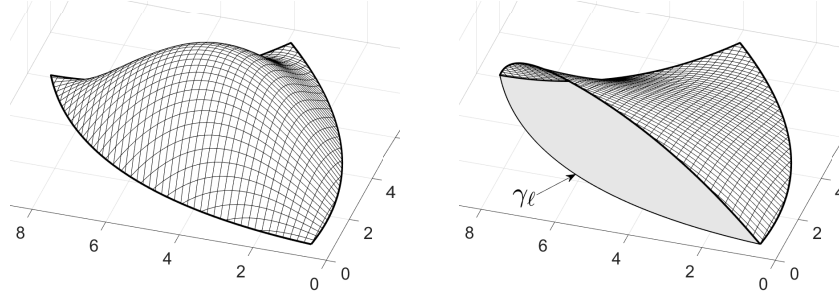
Fig. 1.3 Weights w *(left)* and w_ℓ *(right)*.

When concatenated according to

$$\gamma_{\ell-1}(1) = \gamma_\ell(0), \tag{1.1}$$

these curves form a closed loop without self-intersections. Here and below, the index ℓ always runs from 1 through L and is understood modulo L. Let

$$\sigma_\ell := \gamma_\ell(0) \quad \text{and} \quad \Gamma_\ell := \{\gamma_\ell(u) : 0 \le u < 1\},$$

denote the *corners* and *boundary segments* of Γ, respectively. Formally, the endpoint $\gamma_\ell(1)$ is missing in the definition of Γ_ℓ to obtain a disjoint union $\partial\Gamma = \bigcup_\ell \Gamma_\ell$ for the boundary of Γ. Accordingly, for each boundary point $\beta \in \partial\Gamma$, there exist unique values ℓ and $u \in [0,1)$ such $\beta = \gamma_\ell(u)$.

The building blocks for the construction of the surface **a** are the following:

- Let $\kappa_\ell := [p_\ell, q_\ell] : \mathbb{R}^2 \to \mathbb{R}^2$ be functions that define trimming curves γ_ℓ in the sense of Definition 1 according to the setting described above.
- Let $w : \mathbb{R}^2 \to \mathbb{R}$ be an implicit representation of all trimming curves. That is,

$$w \circ \gamma_j = 0, \quad j = 1, \dots, L.$$

  Further, it is assumed that w is positive on the interior of Γ, see Figure 1.3 *(left)*.
- For each ℓ, let $w_\ell : \mathbb{R}^2 \to \mathbb{R}^2$ be an implicit representation of all trimming curves but γ_ℓ. That is,

$$w_\ell \circ \gamma_j = 0, \quad j = 1, \dots, \ell - 1, \ell + 1, \dots, L.$$

  Further, it is assumed that w_ℓ is non-negative on Γ, and that the only zeros of the sum $\sum_\ell w_\ell$ in Γ are the corners, see Figure 1.3 *(right)*.
- Let $\mathbf{b} : \mathbb{R}^2 \to \mathbb{R}^3$ be a surface, called the *base*. Unit normal and curvature tensor of $\mathbf{b}$ are denoted by $\mathbf{n_b}$ and $E_{\mathbf{b}}$, respectively.
- For $\ell = 1, \dots, L$, let $\mathbf{r}_\ell : \mathbb{R}^2 \to \mathbb{R}^3$ be surfaces, called *ribbons*. Unit normal and curvature tensor of $\mathbf{r}_\ell$ are denoted by $\mathbf{n}_\ell$ and E_ℓ, respectively.

With these ingredients, we construct a new surface that combines base and ribbons in a specific way:

Definition 2 The *ABC-surface* $\mathbf{a} : \Gamma \to \mathbb{R}^3$ corresponding to the data $\mathbf{b}, \mathbf{r}_\ell, w, w_\ell, \kappa_\ell$, as defined above, is given by

$$\mathbf{a} := \frac{w \cdot \mathbf{b} + \sum_{\ell=1}^{L} w_\ell \cdot \mathbf{r}_\ell \circ \kappa_\ell}{w + \sum_{\ell=1}^{L} w_\ell}. \tag{1.2}$$

At corners, where the right hand side is not yet well defined, let

$$\mathbf{a}(\sigma_\ell) := \mathbf{r}_\ell(0,0), \quad \ell = 1, \ldots, L.$$

For the sake of simplicity, this definition is restricted to the case that the domain Γ is simply connected and has always L corners and boundary segments. Generalizations to multiply-connected domains and to disc-like surfaces bounded by one smooth, periodic curve will be discussed in a forthcoming report.

Two basic elements characterize the construction in the definition above. First, the functions κ_ℓ, which define the trimming curves, are used as *reparametrizations* for the ribbons $\mathbf{r}_\ell$ to adapt them to the otherwise unrelated base $\mathbf{b}$. Second, near the boundary segment Γ_j the various implicit representations w and w_ℓ are used as *weights* to fade out the influence of the base $\mathbf{b}$ and all ribbons $\mathbf{r}_\ell$ except for $\mathbf{r}_j$. The ribbon $\mathbf{r}_j$ becomes dominant and determines the shape of $\mathbf{a}$. Thus, the construction provides *accurate boundary control* for $\mathbf{a}$, giving rise to the acronym *ABC-surface*. For a more detailed assessment of this raw idea, we need a further definition:

Definition 3 Let $\mathbf{a}$ be an ABC-surface according to Definition 2. It has *contact order* k at the boundary segment Γ_j if for any $\sigma = \gamma_j(u) \in \Gamma_j$ it holds

$$\bar{w}(\tau) := \frac{w(\sigma + \tau)}{w_j(\sigma + \tau)} = O(|\tau|^{k+1})$$

and, unless $\ell = j$ or $\sigma = \sigma_j$ and $\ell = j - 1$, also

$$\bar{w}_\ell(\tau) := \frac{w_\ell(\sigma + \tau)}{w_j(\sigma + \tau)} = O(|\tau|^{k+1}).$$

Further introducing the notation

$$\bar{\mathbf{r}}_\ell(\tau) := \mathbf{r}_\ell(\kappa_\ell(\sigma + \tau))$$

for the reparametrized ribbons, $\mathbf{a}$ can be written in the form

$$\mathbf{a}(\sigma + \tau) = \frac{\bar{w}(\tau)\mathbf{b}(\sigma + \tau) + \sum_\ell \bar{w}_\ell(\tau)\bar{\mathbf{r}}_\ell(\tau)}{\bar{w}(\tau) + \sum_\ell \bar{w}_\ell(\tau)}. \tag{1.3}$$

Here and below, the variable σ is always assumed to be fixed and mostly omitted in the notation for the sake of simplicity. Unit normal $\bar{\mathbf{n}}_\ell$ and curvature tensor $\bar{E}_\ell$ of

7

$\bar{\mathbf{r}}_\ell$ coincide with the respective quantities of $\mathbf{r}_\ell$ since these surfaces are related by reparametrization,

$$\bar{\mathbf{n}}_\ell(\tau) = \mathbf{n}_\ell(\kappa_\ell(\sigma + \tau)), \quad \bar{E}_\ell(\tau) = E_\ell(\kappa_\ell(\sigma + \tau)). \tag{1.4}$$

In the interior of Γ, $\mathbf{a}$ is a blend of smooth surfaces and thus can be expected to be smooth, too. As always, exceptions may occur in case of an incidental loss of regularity. We will not discuss such degenerate cases, but focus on the behavior of $\mathbf{a}$ at the boundary. The following three theorems clarify the situation:

Theorem 1 (G^0-**boundary**) *Consider an ABC-surface* $\mathbf{a}$ *according to Definition 2 with contact order* $k = 0$ *at* Γ_j. *If the ribbons are consistent according to*

$$\mathbf{r}_{j-1}(1,0) = \mathbf{r}_j(0,0),$$

then $\mathbf{a}$ *is continuous at* Γ_j, *and it holds*

$$\mathbf{a}(\gamma_j(u)) = \mathbf{r}_j(u,0), \quad u \in [0,1]. \tag{1.5}$$

In the following proofs, it is convenient to use the abbreviations

$$h(\tau) := \frac{1}{1 + \bar{w}_{j-1}(\tau)} = \frac{w_j(\sigma_j + \tau)}{w_{j-1}(\sigma_j + \tau) + w_j(\sigma_j + \tau)}, \quad h'(\tau) := 1 - h(\tau),$$

to expand $\mathbf{a}$ in a vicinity of the corner σ_j. Since weights are assumed to be nonnegative, it is $h(\tau) \in [0,1]$. For contact order $k = r - 1$, we obtain

$$\begin{aligned}
\mathbf{a}(\sigma_j + \tau) &= \frac{\bar{\mathbf{r}}_j(\tau) + \bar{w}_{j-1}(\tau)\bar{\mathbf{r}}_{j-1}(\tau) + O(|\tau|^r)}{1 + \bar{w}_{j-1}(\tau) + O(|\tau|^r)} \\
&= h(\tau)\bar{\mathbf{r}}_j(\tau) + h'(\tau)\bar{\mathbf{r}}_{j-1}(\tau) + O(|\tau|^r). \tag{1.6}
\end{aligned}$$

==**Proof**== Consider the point $\sigma = \gamma_j(u) \in \Gamma_j$ and $\mathbf{a}$ in the form (1.3). ==We note that $\bar{\mathbf{r}}_j(\tau) = \mathbf{r}_j(u,0) + O(|\tau|)$== and, by consistency, $\bar{\mathbf{r}}_{j-1}(\tau) = \mathbf{r}_j(0,0) + O(|\tau|)$. For $u > 0$, (1.5) follows from

$$\mathbf{a}(\sigma + \tau) = \frac{\bar{\mathbf{r}}_j(\tau) + O(|\tau|)}{1 + O(|\tau|)} = \bar{\mathbf{r}}_j(\tau) + O(|\tau|) = \mathbf{r}_j(u,0) + O(|\tau|).$$

For $u = 0$, (1.6) yields

$$\mathbf{a}(\sigma + \tau) = h(\tau)\bar{\mathbf{r}}_j(\tau) + h'(\tau)\bar{\mathbf{r}}_{j-1}(\tau) + O(|\tau|) = \mathbf{r}_j(0,0) + O(|\tau|).$$

In the following, $\partial_1 f, \partial_2 f$ denote the partial derivatives of the bivariate function $f : \mathbb{R}^2 \to \mathbb{R}^n$, respectively. $Df := [\partial_1 f\ \partial_2 f] : \mathbb{R}^2 \to \mathbb{R}^{n \times 2}$ denotes the Jacobian.

Theorem 2 (G^1-**boundary**) *Consider an ABC-surface* $\mathbf{a}$ *according to Definition 2 with contact order* $k = 1$ *at* Γ_j. *If the conditions of Theorem 1 are satisfied, if the unit normals of ribbons are consistent according to*

8

$$\mathbf{n}_{j-1}(1,0) = \mathbf{n}_j(0,0),$$

and if the regularity condition

$$\operatorname{rank}(tD\bar{\mathbf{r}}_j(0) + (1-t)D\bar{\mathbf{r}}_{j-1}(0)) = 2 \tag{1.7}$$

is satisfied for all $t \in [0,1]$, then $\mathbf{a}$ has a well-defined unit normal $\mathbf{n_a}$ at Γ_j, and it holds

$$\mathbf{n_a}(\gamma_j(u)) = \mathbf{n}_j(u,0), \quad u \in [0,1]. \tag{1.8}$$

Proof Analogous to the previous proof, we obtain for $u > 0$

$$\mathbf{a}(\sigma + \tau) = \frac{\bar{\mathbf{r}}_j(\tau) + O(|\tau|^2)}{1 + O(|\tau|^2)} = \bar{\mathbf{r}}_j(\tau) + O(|\tau|^2).$$

Differing only by second order terms, the surfaces $\mathbf{a}(\sigma + \cdot)$ and $\bar{\mathbf{r}}$ have the same normal at the origin. Hence, using (1.4), we obtain

$$\mathbf{n_a}(\sigma) = \bar{\mathbf{n}}_j(0) = \mathbf{n}_j(u,0).$$

Below, we mostly omit not only notating σ, but also the argument τ. For $u = 0$, corresponding to the case $\sigma = \sigma_j$, (1.6) yields the derivative

$$D\mathbf{a}(\sigma_j + \tau) = hD\bar{\mathbf{r}}_j + h'D\bar{\mathbf{r}}_{j-1} + (\bar{\mathbf{r}}_j - \bar{\mathbf{r}}_{j-1})Dh + O(|\tau|).$$

By consistency of ribbons, it is $\bar{\mathbf{r}}_j - \bar{\mathbf{r}}_{j-1} = O(|\tau|)$ so that

$$D\mathbf{a}(\sigma_j + \tau) = hD\bar{\mathbf{r}}_j(0) + h'D\bar{\mathbf{r}}_{j-1}(0) + O(|\tau|).$$

Let us consider the leading matrix, defined by the first two summands. Since $h \in [0,1]$, it is a convex combination of $D\bar{\mathbf{r}}_j(0)$ and $D\bar{\mathbf{r}}_{j-1}(0)$. By the regularity condition, it has rank 2, and by consistency of normal vectors, both columns are perpendicular to $\mathbf{n}_j(0,0)$. Hence, normalizing the cross product of these columns and passing to the limit $\tau \to 0$ yields $\mathbf{n_a}(\sigma_j) = \mathbf{n}_j(0,0)$, as stated. Clearly, in general, the derivative $D\mathbf{a}(\sigma_j + \tau)$ itself does not possess a limit for $\tau \to 0$. □

We note that the regularity condition (1.7) is purely technical and typically satisfied. It rules out a degenerate situation, which can occur in a similar way anywhere in any common surface modeling system for an unfortune choice of control data.

The crucial conditions for the existence of normal vectors at the boundary are *algebraic* (proper decay of the functions $\bar{w}$ and $\bar{w}_\ell$) and *geometric* (consistency of ribbons and normals). Similar conditions appear in the following theorem concerning curvature tensors. However, and this may be unexpected, also a *parametric* condition (consistency of derivatives of ribbons) has to be met to guarantee existence of a curvature tensor at corners.

Theorem 3 (G^2-**boundary**) *Consider an ABC-surface $\mathbf{a}$ according to Definition 2 with contact order $k = 2$ at Γ_j. If the conditions of theorems 1 and 2 are satisfied, if the curvature tensors of ribbons are consistent according to*

$$E_{j-1}(1,0) = E_j(0,0),$$

and if the condition

$$D\bar{\mathbf{r}}_{j-1}(0) = D\bar{\mathbf{r}}_j(0) \tag{1.9}$$

is satisfied, then $\mathbf{a}$ *has a well-defined curvature tensor* $E_{\mathbf{a}}$ *at* Γ_j, *and it holds*

$$E_{\mathbf{a}}(\gamma_j(u)) = E_j(u,0), \quad u \in [0,1]. \tag{1.10}$$

Proof As before, we obtain for $u > 0$

$$\mathbf{a}(\sigma + \tau) = \frac{\bar{\mathbf{r}}_j(\tau) + O(|\tau|^3)}{1 + O(|\tau|^3)} = \bar{\mathbf{r}}_j(\tau) + O(|\tau|^3).$$

Differing only by third order terms, the surfaces $\mathbf{a}(\sigma + \cdot)$ and $\bar{\mathbf{r}}$ have the same curvature tensor at the origin. Hence, using (1.4), we obtain

$$E_{\mathbf{a}}(\sigma) = E_j(0) = E_j(u,0).$$

Analogous to the previous proof, we obtain for $u = 0$, corresponding to the case $\sigma = \sigma_j$,

$$\mathbf{a}(\sigma_j + \tau) = h\bar{\mathbf{r}}_j + h'\bar{\mathbf{r}}_{j-1} + O(|\tau|^3)$$

and, using (1.9),

$$D\mathbf{a}(\sigma_j + \tau) = hD\bar{\mathbf{r}}_j(0) + h'D\bar{\mathbf{r}}_{j-1}(0) + O(|\tau|) = D\bar{\mathbf{r}}_j(0) + O(|\tau|).$$

This time, the derivative has a limit at the corner,

$$D\mathbf{a}(\sigma_j) = D\bar{\mathbf{r}}_j(0). \tag{1.11}$$

The second order partial derivatives are given by

$$\begin{aligned}
\partial_{\mu\nu}\mathbf{a}(\sigma_j + \tau) =&\partial_{\mu\nu}h(\bar{\mathbf{r}}_j - \bar{\mathbf{r}}_{j-1}) + \partial_\mu h\,(\partial_\nu\bar{\mathbf{r}}_j - \partial_\nu\bar{\mathbf{r}}_{j-1}) + \\
&\partial_\nu h\,(\partial_\mu\bar{\mathbf{r}}_j - \partial_\mu\bar{\mathbf{r}}_{j-1}) + h\partial_{\mu\nu}\bar{\mathbf{r}}_j + h'\partial_{\mu\nu}\bar{\mathbf{r}}_{j-1} + O(|\tau|) \\
=&h\partial_{\mu\nu}\bar{\mathbf{r}}_j(0) + h'\partial_{\mu\nu}\bar{\mathbf{r}}_{j-1}(0) + O(|\tau|),
\end{aligned}$$

where we used that $\bar{\mathbf{r}}_{j-1}(0) = \bar{\mathbf{r}}_j(0)$ and $D\bar{\mathbf{r}}_{j-1}(0) = D\bar{\mathbf{r}}_j(0)$. Further, the curvature tensors of $\bar{\mathbf{r}}_{j-1}$ and $\bar{\mathbf{r}}_j$ coincide at the origin, $\bar{E}_{j-1}(0) = \bar{E}_j(0)$. This implies that also the second fundamental forms coincide,

$$\bar{B}_{j-1}^{\mu\nu}(0) := \langle \bar{\mathbf{n}}_{j-1}(0), \partial_{\mu\nu}\bar{\mathbf{r}}_{j-1}(0) \rangle = \langle \bar{\mathbf{n}}_j(0), \partial_{\mu\nu}\bar{\mathbf{r}}_j(0) \rangle =: \bar{B}_j^{\mu\nu}(0).$$

The second fundamental form of $\mathbf{a}$ is

$$B_{\mathbf{a}}^{\mu\nu}(\sigma_j + \tau) := \langle \mathbf{n}_{\mathbf{a}}(\sigma_j + \tau), \partial_{\mu\nu}\mathbf{a}(\sigma_j + \tau) \rangle.$$

10

By Theorem 2, the normal vector of $\mathbf{a}$ converges, i.e., $\mathbf{n_a}(\sigma_j + \tau) = \mathbf{n_a}(\sigma_j) + O(|\tau|)$. Hence, we obtain

$$B_\mathbf{a}^{\mu\nu}(\sigma_j + \tau) = h\langle\mathbf{n_a}(\sigma_j), \partial_{\mu\nu}\bar{\mathbf{r}}_j(0)\rangle + h'\langle\mathbf{n_a}(\sigma_j), \partial_{\mu\nu}\bar{\mathbf{r}}_{j-1}(0)\rangle + O(|\tau|)$$
$$= hB_j^{\mu\nu}(0) + h'B_{j-1}^{\mu\nu}(0) + O(|\tau|) = B_j^{\mu\nu}(0) + O(|\tau|)$$

and finally, using $\mathbf{n_a}(\sigma_j) = \bar{\mathbf{n}}_j(0) = \bar{\mathbf{n}}_{j-1}(0)$,

$$B_\mathbf{a}^{\mu\nu}(\sigma_j) = B_j^{\mu\nu}(0).$$

Together with (1.11) and (1.4), this implies coincidence of curvature tensors,

$$E_\mathbf{a}(\sigma_j) = \bar{E}_j(0) = E_j(0,0),$$

and the proof is complete. $\qquad\qquad\qquad\qquad\qquad\qquad\qquad\qquad\qquad$ □

The proofs of the three theorems show that G^k-properties on the interior part of the boundary segments ($0 < u < 1$) are easily achieved by requesting proper decay of the functions $\bar{w}$ and $\bar{w}_\ell$. Consistency and regularity conditions are requested only to guarantee good behavior at the corners. Remarkably, condition (1.9) concerning consistency of the derivatives of reparametrized ribbons shows that the functions κ_ℓ cannot be chosen independently of the ribbons $\mathbf{r}_\ell$. More precisely, the interrelation

$$D\bar{\mathbf{r}}_{j-1}(0) = D\mathbf{r}_{j-1}(1,0)D\kappa_{j-1}(\sigma_j) = D\mathbf{r}_j(0,0)D\kappa_j(\sigma_j) = D\bar{\mathbf{r}}_j(0) \qquad (1.12)$$

must be observed. Assuming that the ribbons are given and the reparametrizations are still unknown, this equation yields a linear constraint on the pair $D\kappa_{j-1}, D\kappa_j$ at the corner σ_j. Vice versa, if the reparametrizations are given, the space of admissible ribbons is restricted to a linear subspace.

The following example shows that this condition is in fact crucial. Let

$$\bar{\mathbf{r}}_{j-1}(x,y) = \begin{bmatrix} x \\ y \\ x^2 \end{bmatrix}, \quad \bar{\mathbf{r}}_j(x,y) = \begin{bmatrix} 2x \\ 2y \\ 4x^2 \end{bmatrix}, \quad (x,y) \in [0,1]^2.$$

Near the origin, the traces of both surfaces coincide so that consistency of point, normal, and curvature tensor is guaranteed. However,

$$D\bar{\mathbf{r}}_{j-1}(0,0) = \begin{bmatrix} 1 & 0 \\ 0 & 1 \\ 0 & 0 \end{bmatrix} \neq \begin{bmatrix} 2 & 0 \\ 0 & 2 \\ 0 & 0 \end{bmatrix} = D\bar{\mathbf{r}}_j(0,0).$$

The weight functions $w_{j-1}(x,y) = x^3, w_j(x,y) = y^3$ have proper decay at the boundary curves $\gamma_{j-1}(u) = [u,0,0]$ and $\gamma_j(u) = [0,u,0]$. Assuming for simplicity that the base and all other ribbons vanish, we obtain
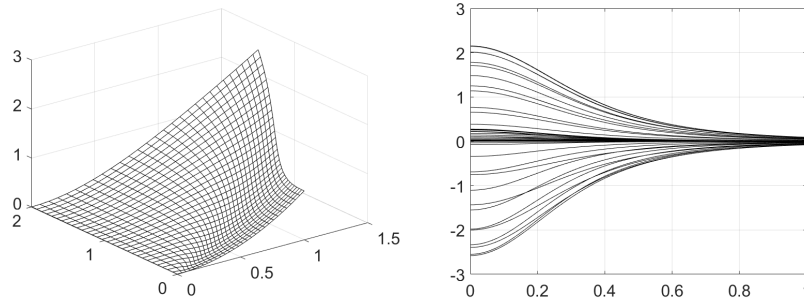
Fig. 1.4 Surface $\mathbf{a}(x, y)$ obtained by blending inappropriately reparametrized ribbons *(left)* and its Gaussian curvature $K(r\cos\varphi, r\sin\varphi)$ plottet over $r \in (0, 1]$ for 30 different angles $\varphi \in [0, \pi/2]$ *(right)*.

$$\mathbf{a}(x,y) = \frac{1}{x^3 + y^3} \begin{bmatrix} x(x^3 + 2y^3) \\ y(x^3 + 2y^3) \\ x^2(x^3 + 4y^3) \end{bmatrix}.$$

Skipping the technical details, we note that

$$\lim_{(x,y)\to(0,0)} \mathbf{a}(x,y) = \bar{\mathbf{r}}_{j-1}(0,0) = \bar{\mathbf{r}}_j(0,0) = \begin{bmatrix} 0 \\ 0 \\ 0 \end{bmatrix}$$

and

$$\lim_{(x,y)\to(0,0)} \mathbf{n_a}(x,y) = \bar{\mathbf{n}}_{j-1}(0,0) = \bar{\mathbf{n}}_j(0,0) = \begin{bmatrix} 0 \\ 0 \\ 1 \end{bmatrix}.$$

However, the curvature tensor $E_\mathbf{a}$ is discontinuous at the origin. Figure 1.4 shows the surface $\mathbf{a}$ *(left)* and the Gaussian curvature $K(r\cos\varphi, r\sin\varphi)$ *(right)* as a function of r. The individual lines correspond to 30 equally spaced angles φ in the interval $[0, \pi/2]$. For $\varphi = 0$ and $\varphi = \pi/2$, corresponding to the trimming curves γ_{j-1} and γ_j, it is $\lim_{r\to 0} K(r,0) = \lim_{r=0} K(0,r) = 0$, as suggested by the cylindrical shape of $\bar{\mathbf{r}}_{j-1}$ and $\bar{\mathbf{r}}_j$. However, other angles yield non-zero limits.

1.3 ABC-spline surfaces

In the previous section, the ABC-principle was introduced in great generality. Our main goal, however, is to find a special embodiment of the setup that is fully compatible with the predominant standard of industrial surface modeling: trimmed NURBS.

To this end, we assume that all building blocks of the ABC-surface $\mathbf{a}$ are tensor product NURBS. Even more, for the sake of simplicity, we consider only purely polynomial, i.e., non-rational splines. Further, it is practical (but not necessary) to use a common set of knot vectors for the base $\mathbf{b}$, the weights w, w_ℓ and the reparametrizations κ_ℓ; degrees may be different. By contrast, the knots of the ribbons $\mathbf{r}_\ell$ are completely independent. It is immediately clear that the concatenation, multiplication, summation and division of piecewise polynomial functions yields a piecewise rational function $\mathbf{a}$. Denoting the coordinate degree of the bivariate spline s by $\deg s \in \mathbb{N}_0^2$ and its total degree by $|\deg s| \in \mathbb{N}_0$, we obtain

$$d := \deg(w\mathbf{b}) = \deg w + \deg \mathbf{b}$$
$$d_\ell := \deg(w_\ell \mathbf{r}_\ell \circ \kappa_\ell) = \deg w_\ell + |\deg \mathbf{r}_\ell| \deg \kappa_\ell.$$

Together, the maximal degree of the rational pieces of $\mathbf{a}$ equals that of the corresponding numerators, and is given by

$$\deg \mathbf{a} = \max\{d, d_1, \ldots, d_L\}, \tag{1.13}$$

where the maximum is taken component-wise. More specific results will be presented later on.

The crucial question that has to be addressed now concerns the construction of suitable splines w, w_ℓ, and κ_ℓ. In recent works [VSVS20, VVSS20], reparametrizations for domains bounded by curves are obtained as solutions to variational problems with the given trimming curves γ_ℓ as boundary conditions. It can be expected that this yields good visual results, but of course, there does not exist a closed-form solution, and much less a spline fulfilling the condition $\kappa_\ell(\gamma(u)) = [u, 0]$. Similar problems arise when seeking weights vanishing at the boundary or parts thereof.

The solution of the problem to find weights and reparametrizations compatible with the boundary is amazingly simple: There is no need to define the boundary curves γ_ℓ explicitly. It suffices to define them *implicitly* by the functions κ_ℓ according to Definition 1,

$$\gamma_\ell(u) := \{\xi \in \mathbb{R}^2 : \kappa_\ell(\xi) = [u, 0]\}.$$

This setting is justified by the fact that standard CAD systems and also standard file exchange formats like STEP or IGES allow trimming curves to be specified explicitly as a closed loop of spline curves in the parametric domain, or alternatively–and this is the option used here–as a closed loop of spline curves in $\mathbb{R}^3$ bounding the trace of the given NURBS surface. By Theorem 1, the curves

$$[0, 1] \ni u \mapsto \mathbf{c}_\ell(u) := \mathbf{r}_\ell(u, 0) = \mathbf{a}(\gamma_\ell(u)), \quad \ell = 1, \ldots, L,$$

can serve exactly that purpose. Actually, the planar trimming curves γ_ℓ need not be computed at any processing step of ABC-spline surfaces as long as geometric trimming by spatial curves, as explaind in Section 4, is available.

Now, we elaborate on methods how to determine suitable reparametrizations κ_ℓ and weights w, w_ℓ under the assumption that the base $\mathbf{b}$ and the ribbons $\mathbf{r}_\ell$ are given.

13

1.3.1 Reparametrization

In principle, the functions κ_ℓ can be chosen quite arbitrarily. Basically, only the consistency condition (1.1) must be satisfied. This means that there exist points $\sigma_\ell \in \mathbb{R}^2$ such that

$$\kappa_\ell(\sigma_\ell) = [0,0], \quad \kappa_{\ell-1}(\sigma_\ell) = [1,0]$$

for all ℓ. If continuity of curvature tensors is requested, also condition (1.12) must be observed, i.e.,

$$D\mathbf{r}_{\ell-1}(1,0) \cdot D\kappa_{\ell-1}(\sigma_\ell) = D\mathbf{r}_\ell(0,0) \cdot D\kappa_\ell(\sigma_\ell). \tag{1.14}$$

Further, to obtain fair surfaces, it is reasonable to request that κ_ℓ reparametrizes $\mathbf{r}_\ell$ in such a way that it is close to the base,

$$\mathbf{r}_\ell \circ \kappa_\ell \approx \mathbf{b}.$$

The simplest way to achieve this (and possibly other desirable properties) is as follows: First, for each ℓ, we consider pairs of parameters $\sigma_\ell, \tau_\ell \in \mathbb{R}^2$, characterized by

$$\mathbf{r}_\ell(\tau_\ell) \approx \mathbf{b}(\sigma_\ell).$$

Collecting a sufficiently large, but finite number of them yields the set K_ℓ. Such pairs $(\sigma_\ell, \tau_\ell) \in K_\ell$ can be found easily by requesting that the line connecting the points $\mathbf{r}_\ell(\tau_\ell)$ and $\mathbf{b}(\sigma_\ell)$ be perpendicular to one of the two surfaces. To address the special role of corners, the set K_ℓ must contain the τ values $\tau_\ell^0 := [0,0]$ and $\tau_\ell^1 := [1,0]$. The corresponding σ-values must be consistent in the sense that the corners

$$\sigma_\ell := \sigma_\ell^0 = \sigma_{\ell-1}^1$$

are well-defined. At this and possibly other data points, the function κ_ℓ should not only approximate but interpolate the prescribed values. More precisely, let $K_\ell' \subset K_\ell$ be the subsets of pairs intended for interpolation and $K_\ell'' := K_\ell \setminus K_\ell'$ the remainders. In particular, the pairs $(\sigma_\ell^0, \tau_\ell^0)$ and $(\sigma_\ell^1, \tau_\ell^1)$ addressing the corners belong to K_ℓ'. Now, the conditions to be satisfied by κ_ℓ are

$$\kappa_\ell(\sigma_\ell) = \tau_\ell, \quad (\sigma_\ell, \tau_\ell) \in K_\ell'$$
$$\kappa_\ell(\sigma_\ell) \approx \tau_\ell, \quad (\sigma_\ell, \tau_\ell) \in K_\ell''.$$

Standard techniques, including all kinds of least squares methods or smoothing splines can be used to select κ_ℓ accordingly from a given space of splines. If the problem is overconstrained in the sense that no solution exists, the spline space must be enlarged or the conditions must be relaxed. Conversely, if the solution is not unique, the spline space must be reduced or more conditions must be specified.

The interpolation conditions $\kappa_\ell(\sigma_\ell) = [0,0]$ and $\kappa_{\ell-1}(\sigma_\ell) = [1,0]$ for the corners yield

$$\gamma_\ell(0) = \gamma_{l-1}(1) = \sigma_\ell,$$

as requested by (1.1). Still, condition (1.14) needs to be addressed. When needed, one determines matrices $T_\ell \in \mathbb{R}^{3\times 2}$ such that

$$T_\ell \approx D\mathbf{b}(\sigma_\ell), \quad \mathbf{n}_\ell(0,0)^{\mathrm{t}} \cdot T_\ell = 0, \quad \ell = 1,\dots,L.$$

In particular, the columns of T_ℓ span the wanted tangent space at σ_ℓ. Now, κ_ℓ is determined as before, but such that is satisfies the additional conditions

$$D\mathbf{r}_\ell(0,0) \cdot D\kappa_\ell(\sigma_\ell) = T_\ell$$
$$D\mathbf{r}_\ell(1,0) \cdot D\kappa_\ell(\sigma_{\ell+1}) = T_{\ell+1}.$$

As the chain rule shows, this is in accordance with $\mathbf{r}_\ell \circ \kappa_\ell \approx \mathbf{b}$, and it also implies (1.14).

1.3.2 Weights

Once the reparametrizations $\kappa_\ell = [p_\ell, q_\ell]$ are known, also suitable weights w and w_ℓ can be determined conveniently.

By definition, the second coordinate q_ℓ of κ_ℓ vanishes at γ_ℓ. Assuming that the ABC-surface $\mathbf{a}$ to be determined should have contact order $k_\ell \geq 0$ at the boundary segment Γ_ℓ, the simplest choice for w is

$$w = q_1^{r_1} \cdots q_L^{r_L}, \tag{1.15}$$

where the exponents are $r_\ell := k_\ell + 1$. At this point, it has to be made sure that each factor q_ℓ is positive on $\Gamma \setminus \Gamma_\ell$. Additional zeros away from Γ_ℓ are not critical. Increasing some control points of B-splines vanishing at that boundary segment, these zeros can be removed without changing the crucial boundary behavior. However, zeros near the boundary may be persistent so that the whole construction fails. In particular, reentrant corners are likely to cause such a situation. This case requires a special treatment and will be discussed in a forthcoming report.
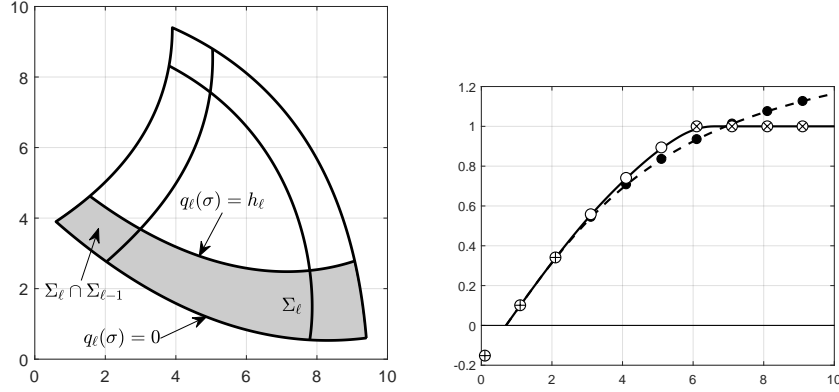
Omitting one factor yields possible weights

$$w_\ell = q_1^{r_1} \cdots q_{\ell-1}^{r_{\ell-1}} q_{\ell+1}^{r_{\ell+1}} \cdots q_L^{r_L}.$$

Let us check the conditions concerning contact order given in Definition 3. For $\sigma \in \Gamma_j$, we obtain

$$\bar{w}(\tau) = \frac{w(\sigma + \tau)}{w_j(\sigma + \tau)} = q_j^{r_j}(\sigma + \tau) = O(|\tau|^{r_j})$$

since $q_j(\sigma) = 0$. Further,

Fig. 1.5 Boundary stripes *(left)* and univariate plateau generation with original control points •, unchanged control points ⊕, constant control points ⊗, and optimized control points ○ *(right)*.

$$\bar{w}_\ell(\tau) = \frac{w_\ell(\sigma + \tau)}{w_j(\sigma + \tau)} = \frac{q_j^{r_j}(\sigma + \tau)}{q_\ell^{r_\ell}(\sigma + \tau)} = O(|\tau|^{r_j})$$

unless the denominator vanishes at σ, and this is only possible if $\ell = j$ or $\ell = j - 1$ and $\sigma = \sigma_j$. Exactly these cases are excluded in the definition.

The weights suggested above have two drawbacks: First, the influence of each ribbon extends over the whole surface, which might be unwanted. Second, the polynomial degree of such weights is increasing with L. If, for example, $L = 6$, $\deg q_\ell = [3,3]$, and $r_\ell = 3$ for all ℓ to achieve contact order $k = 2$ everywhere, then $\deg w = \sum_{\ell=1}^{L} r_\ell \deg q_\ell = [54,54]$. This might cause problems with efficiency of storage and speed of evaluation after converting the surface **a** from its procedural definition (1.2) to the usual form

$$\mathbf{a} = \frac{\sum_i \omega_i b_i \mathbf{p}_i}{\sum_i \omega_i b_i}$$

of a NURBS surface, i.e., the linear combination of control points $\mathbf{p}_i$ by means of B-splines b_i and (constant) weights ω_i. The latter is requested in particular for the export of **a** to standard file formats, as addressed in the next section. The following modification of weights away from the boundary of the domain Γ solves both issues:

Denote by

$$\Sigma_\ell := \{\sigma \in \Gamma : q_\ell(\sigma) \le h_\ell\}$$

the *boundary stripes* of Γ with *width* h_ℓ. The widths $h_\ell > 0$ are assumed to be chosen small enough to make sure that only boundary stripes of neighboring curves intersect, and that these intersections as well as the stripes themselves consist of a single connected piece, see Figure 1.5 *(left)*. Now, we derive from q_ℓ a new spline $\bar{q}_\ell$ as follows: First, classify the indices in the B-spline representation $q_\ell = \sum_i q_\ell^i b_i$ according to
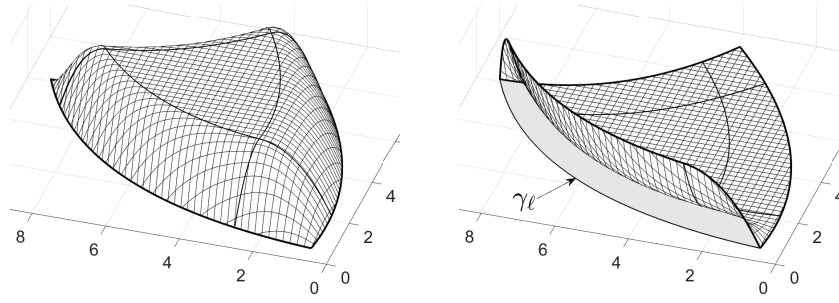
Fig. 1.6 Weights w *(left)* and w_ℓ *(right)* with plateau.

$$I_\ell := \{i : q_\ell(\sigma) = 0 \text{ for some } \sigma \in \operatorname{supp} b_i\}$$
$$J_\ell := \{i : q_\ell(\sigma) > h_\ell \text{ for some } \sigma \in \operatorname{supp} b_i\}.$$

That is, B-splines b_i affect the boundary if $i \in I_\ell$, and they affect the part beyond the boundary stripe if $i \in J_\ell$. Second, if the sets I_ℓ and J_ℓ are not disjoint, refine the B-spline representation of q_ℓ by knot insertion and repeat the first step. Third, set

$$\bar{q}_\ell^i := \begin{cases} q_\ell^i & \text{if } i \in I_\ell \\ h_\ell & \text{if } i \in J_\ell. \end{cases} \tag{1.16}$$

Coefficients with indices neither in I_ℓ nor in J_ℓ are determined such that the resulting spline has reasonable shape, for instance by minimizing a standard fairness functional. Fourth, define the spline $\bar{q}_\ell := \sum_i \bar{q}_\ell^i b_i$. By construction, $\bar{q}_\ell$ is an implicit representation of γ_ℓ, but has a *plateau* with constant value h_ℓ beyond the boundary stripe Σ_ℓ. Figure 1.5 *(right)* illustrates the procedure exemplarily in the univariate case. Replacing (1.15) by

$$w = \bar{q}_1^{r_1} \cdots \bar{q}_L^{r_L},$$

we obtain an implicit representation of $\partial \Gamma$ with plateau on the interior part of the domain that is not covered by a boundary stripe, see Figure 1.6 *(left)*. By construction, the coordinate degree of w is bounded by

$$\deg w \le \max_\ell (r_\ell \deg q_\ell + r_{\ell+1} \deg q_{\ell+1})$$

since at any given point $\sigma \in \Gamma$ at most two factors are non-constant. Notably, the degree does not depend on the number L of boundary segments. In the example above, we have now $\deg q = [18, 18]$. This is still a relatively high degree, but much less than before, and can be considered manageable.

The weights w_ℓ may be modified in a similar spirit. We define the functions

$$\hat{q}_\ell := \bar{q}_{\ell-1} \bar{q}_{\ell+1}$$

17

and process them exactly like the functions q_ℓ above, but now replacing (1.16) by

$$\tilde{q}_\ell^i := \begin{cases} \hat{q}_\ell^i & \text{if } i \in I_\ell \\ 0 & \text{if } i \in J_\ell. \end{cases}$$

This way, we produce a function with a zero plateau beyond the boundary stripe. The desired weight is now simply given by

$$w_\ell := \tilde{q}_\ell^{r_\ell},$$

see Figure 1.6 *(right)*. The degree

$$\deg w_\ell = r_\ell \max(\deg q_{\ell-1}, \deg q_{\ell+1})$$

is again independent of L.

Let us reconsider the degree of **a** for weights w and w_ℓ with plateau, as defined above. For simplicity, we assume that $\deg \mathbf{b} = \deg \kappa_\ell = [n,n]$ and $\deg \mathbf{r}_\ell = [n,m]$, and that all contact orders are equal to $k = r - 1$. Then, using (1.13),

$$\deg \mathbf{a} = [n,n] \cdot \max\{2r+1, r+n+m\}.$$

The coordinate degree of the ribbons is set to the unmatched pair $[n,m]$ for the following reason: In the first direction, corresponding to the behavior along the boundary, full flexibility concerning the choice of knots and degrees is provided to model a large variety of shapes. By contrast, in the second direction, corresponding to the behavior transversal to the boundary, it is sufficient to deal with pure polynomials of low degree. For instance, choosing $m = 1$ allows the definition of the boundary curves $\mathbf{r}_\ell(u,0)$ and the boundary normals $\mathbf{n}_\ell(u,0)$ along Γ_ℓ. When also the curvature tensors $E_\ell(u,0)$ shall be prescribed, it suffices to choose $m = 2$. The minimal configuration yielding a G^1-patch and contact order $k = 1$ requests $n = 2$ and $m = 1$, leading to $\deg \mathbf{a} = [10,10]$. For a G^2-patch and contact order $k = 2$, one chooses at least $n = 3$ and $m = 2$ to obtain $\deg \mathbf{a} = [24,24]$.

Modeling with surfaces of such a high degree is commonly considered to be impractical. However, this is never requested. The geometric building blocks–base and ribbons–can be assumed to be splines of low degree, and their control points can be manipulated (manually or automatically) as usual. The conversion of the ABC-surface **a** to NURBS form

$$\mathbf{a} = \frac{\sum_i \omega_i b_i \mathbf{p}_i}{\sum_i \omega_i b_i},$$

as detailed in the next section, serves only the purpose to prepare it for file export according to industrial standards. It should be considered as a *read-only representation*, to be used for evaluation purposes. Never ever, the control points $\mathbf{p}_i$ should be touched again after being derived from (1.2).

1.4 File export

As a matter of fact, data exchange between industrial CAD/CAM systems is limited to a few completely standardized file formats, like IGES or STEP. The only type of surfaces commonly available therein are trimmed NURBS. Other modeling paradigms, say based on box splines, exponential splines, or subdivision are typically not supported. For the trimming of a NURBS surface $\mathbf{s} : \mathbb{R}^2 \to \mathbb{R}^3$, the following three options can be assumed to be available:

Parametric trimming. A closed loop of planar spline curves $\gamma_1, \ldots, \gamma_L$ without self-intersections is specified. The compact set $\Gamma \subset \mathbb{R}^2$ bounded by these curves is used as the domain of the trimmed surface $\mathbf{s}$.

Geometric trimming. A closed loop of spatial spline curves $\mathbf{c}_1, \ldots, \mathbf{c}_L$ is specified. Since it cannot be assumed that the traces of these curves are contained in the surface, the corresponding planar curves are defined by $\gamma_\ell(u) := \alpha$ where $\alpha \in \mathbb{R}^2$ is chosen such that $\mathbf{s}(\alpha) \approx \mathbf{c}_\ell(u)$ with the help of some projection method. These curves γ_ℓ need not be splines by themselves, but are computed numerically. They are merely assumed to form a closed loop, which is bounding the domain Γ.

Hybrid trimming. Some segments of the boundary are defined by planar spline curves, and the other ones by spatial spline curves. The planar curves together with the preimages of the projected spatial curves are assumed to form a closed loop, which is bounding the domain Γ.

As we have seen, ABC-spline surfaces are piecewise rational. But nevertheless, in general, they cannot be represented as trimmed NURBS in the requested way. The point is that the summands $\mathbf{r}_\ell \circ \kappa_\ell$ may produce inner boundaries between rational segments that are not axis-aligned in the parameter domain and hence cannot be understood as knot lines. To solve this issue, we present a special construction of the reparametrizations κ_ℓ that leads to a situation where $\mathbf{a}$ can be represented as the union of separate parts, each of which is a genuine trimmed NURBS surface with boundary segments given either geometrically by a 3d spline curve or parametrically by a 2d spline curve.

For a spline s of degree n with knot vector $U = [u^0, \ldots, u^N]$, the natural domain of definition is the interval $[u^n, u^{N-n}]$. We assume that s can be evaluated on all of $\mathbb{R}$ by simply prolonging the leftmost polynomial piece from $[u^n, u^{n+1}]$ to $(-\infty, u^{n+1}]$ and the rightmost piece from $[u^{N-n-1}, u^{N-n}]$ to $[u^{N-n-1}, \infty)$. Hence, true break points, where higher order derivatives are discontinuous, appear only at the *inner knots $u^{n+1}, \ldots, u^{N-n-1}$*.

Denote the knot vectors of $\mathbf{r}_\ell$ by U_ℓ, V_ℓ. We start with considering the second vector V_ℓ. Critical points $\sigma \subset \mathbb{R}^2$ that are mapped to the knot line $\mathbb{R} \times \{v_\ell^j\}$ for some inner knot $v_\ell^j \in V_\ell$ by the reparametrization $\kappa_\ell = [p_\ell, q_\ell]$ are characterized by

$$q_\ell(\sigma) = v_\ell^j.$$

In general, neither the levelsets of q_ℓ nor their images under $\mathbf{r}_\ell$ are splines. Special constructions for q_ℓ to create such a situation are possible, but impractical. It is much easier and completely sufficient to request that V_ℓ does not possess any inner
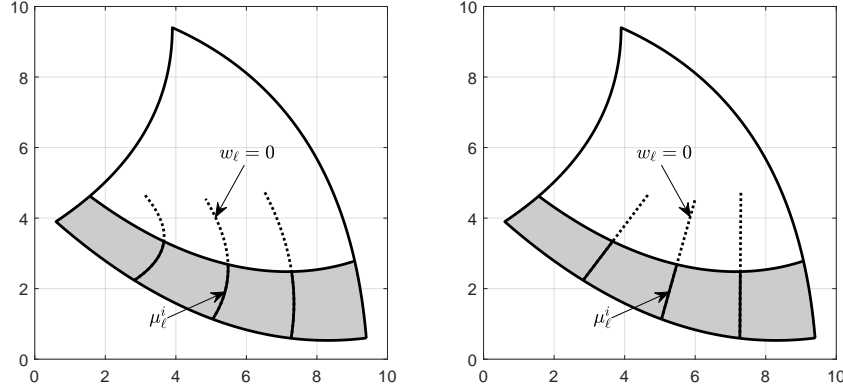
Fig. 1.7 Genral *(left)* and straight *(right)* levelsets μ_ℓ^i.

knots at all. For instance, we may assume $V_\ell = [0, \ldots, 0, 1, \ldots, 1]$, what is just the knot vector for polynomials in Bézier form. We identified this setting already at the end of the preceding section as a legitimate choice. To sum up, ribbons that are pure polynomials in the second coordinate are able to carry information on location, unit normal, and curvature tensor along the boundary curve, and they do not have breaks in the second coordinate.

The treatment of the first variable is more involved since assuming also this dependence to be purely polynomial would unduly restrict the variety of shapes that can be modeled. Critical points $\sigma \subset \mathbb{R}^2$ that are mapped to the inner knot $u_\ell^i \in U_\ell$ by κ_ℓ are characterized by

$$p_\ell(\sigma) = u_\ell^i.$$

This time, it is appropriate to demand that the critical levelsets of p_ℓ corresponding to inner knots of U_ℓ are linear. More precisely, let

$$\mu_\ell^i := \{\sigma \in \Gamma : p_\ell(\sigma) = u_\ell^i \text{ and } w_\ell(\sigma) > 0\}$$

denote the relevant parts of the levelsets of p_ℓ corresponding to the knots u_ℓ^i. In general, these curves are bent, see Figure 1.7 *(left)*, but p_ℓ can be determined such that they become straight lines, see Figure 1.7 *(right)*. One may proceed as follows:

First, for each knot $u_\ell^i \in U_\ell$, choose a direction $\delta_\ell^i \in \mathbb{R}^2$ such that

$$\mathbf{r}_\ell(u_\ell^i, t) \approx \mathbf{b}(\gamma_\ell(u_\ell^i) + t\delta_\ell^i)$$

for arguments $\gamma_\ell(u_\ell^i) + t\delta_\ell^i$ within the boundary stripe Σ_ℓ. Denoting by $D\mathbf{b}^+ := (D\mathbf{b}^T D\mathbf{b})^{-1}D\mathbf{b}^T$ the pseudo-inverse of the Jacobian $D\mathbf{b}$, one may set in particular

$$\delta_\ell^i := D\mathbf{b}^+(\gamma_\ell(u_\ell^i)) \cdot \partial_2\mathbf{r}_\ell(u_\ell^i, 0).$$

20
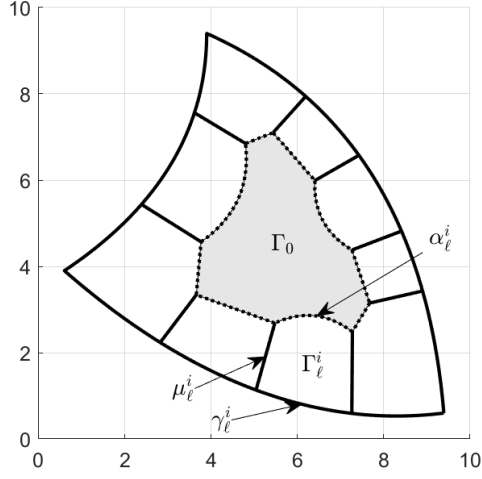
Fig. 1.8 Partition of the domain Γ into pieces ready for file export.

Second, define the line segment

$$\mu_\ell^i := \{\gamma_\ell^i + t\delta_\ell^i : t \in \mathbb{R}\} \cap \Sigma_\ell$$

with direction δ_ℓ^i within the boundary stripe Σ_ℓ. Third, choose sufficiently many pairs of points (σ_ℓ, τ_ℓ) of the form

$$\sigma_\ell = \gamma_\ell(u_\ell^i) + t\delta_\ell^i \in \mu_\ell^i, \quad \tau_\ell = (u_\ell^i, t)$$

and add them to the set K_ℓ' of data to be interpolated.

Using this setup, points $\sigma \in \Gamma$ that are mapped to the inner knot u_ℓ^i of $\mathbf{r}_\ell$ by p_ℓ either lie on the straight line μ_ℓ^i or are irrelevant since $w_\ell(\sigma) = 0$.

Assuming that the ribbons $\mathbf{r}_\ell$ are polynomials in the second variable and that the level sets μ_ℓ^i are straight, as described, we can partition the domain Γ into an interior part Γ_0 and boundary parts Γ_ℓ^i by a network of curves, consisting of three different types: First, there are the segments γ_ℓ^i of the trimming curves γ_ℓ corresponding to intervals between consecutive knots in U_ℓ. Second, there are the level sets μ_ℓ^i, and third, there are auxiliary spline curves α_ℓ^i, to be chosen at will, connecting the endpoints of the level sets. Figure 1.8 illustrates the setting. Restricting the ABC-surface $\mathbf{a}$ to the subdomains Γ_0, Γ_ℓ^i yields pieces $\mathbf{a}_0, \mathbf{a}_\ell^i$, respectively, which are trimmed NURBS surfaces ready for filing with standard data formats. They do not have interior breaks aside from a regular knot grid, and their boundaries are formed by spatial spline curves $\mathbf{a} \circ \gamma_\ell^i$ and planar spline curves $\mu_\ell^i, \alpha_\ell^i$.
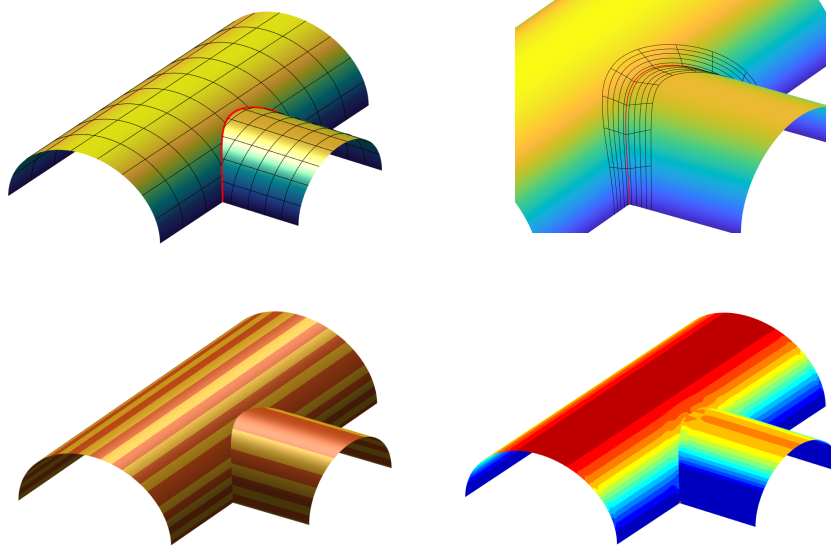
Fig. 1.9 Two intersecting cylinders – paramatric lines *(top left)*, ribbons near intersection curve *(top right)*, isophotes *(bottom left)*, and mean curvature shading *(bottom right)*.

1.5 Examples

The focus of this article is on theory, but still, skipping many technical details, we want to present three examples to illustrate the potential of our approach. They show in turn composite surfaces with G^0, G^1, and G^2 contact according to theorems 1, 2, and 3, respectively. All surfaces, reparametrizations, and weights are bicubic tensor product splines; all weights are used in the version with plateau.

Figure 1.9 presents a typical example from solid modeling: two intersecting cylinders that trim each other. The first plot shows two ABC-surfaces $\mathbf{a}^1, \mathbf{a}^2$ together with a few parameter lines, which follow the given shapes in the natural way. The spline representations $\mathbf{b}^1, \mathbf{b}^2$ of the two original cylinders serve as bases for $\mathbf{a}^1, \mathbf{a}^2$, respectively. The second plot shows the pair of ribbons $\mathbf{r}^1, \mathbf{r}^2$ used to model the region near the intersection curve. Both ribbons have 9 interior knots in longitudinal direction. Their parametrizations are adapted to the local situation and chosen such that they share a common curve $\mathbf{c} = \mathbf{r}^1(\cdot, 0) = \mathbf{r}^2(\cdot, 0)$. This curve approximates the exact intersection $\mathbf{b}^1 \cap \mathbf{b}^2$ of the two original cylinders with high accuracy. The watertight connection of ribbons is easy to achieve by coinciding boundary control points since both ribbons are in Bézier form in transversal direction. Theorem 1 says that this property is inherited by the two ABC-surfaces, i.e., they also join seemlessly at $\mathbf{c}$. The third plot shows the impeccable pattern of isophotes, while the fourth one is colored by mean curvature. Only here, one can see that the two surfaces $\mathbf{a}^1, \mathbf{a}^2$
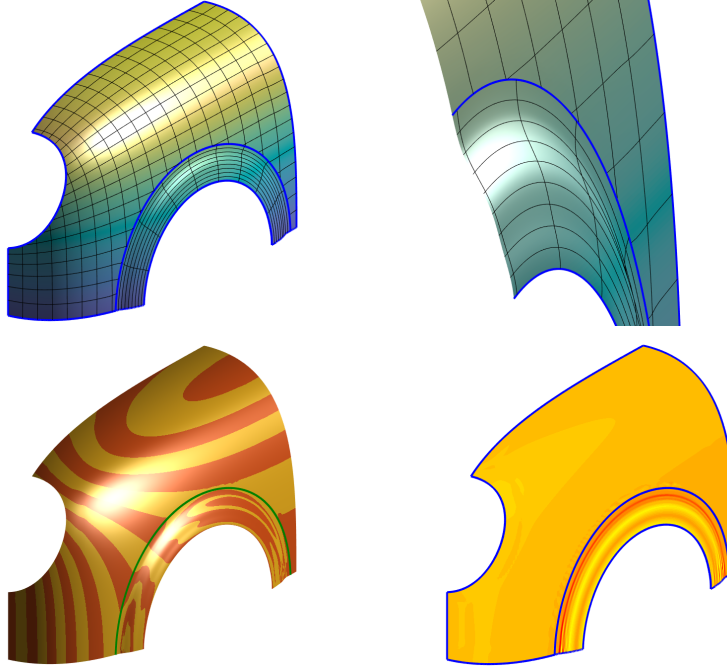
Fig. 1.10 Fender of a fictional car – whole composite surface *(top left)*, zoom on cross section *(top right)*, isophotes *(bottom left)*, and mean curvature shading *(bottom right)*.

slightly deviate from the perfect cylindrical shape of the original surfaces. This deviation could be made arbitrarily small by choosing finer knot sequences. However, as a matter of fact, it is impossible to do without any deviation since the exact intersection of the original cylinders cannot be represented by a spline curve–neither in geometry space nor in the parametric domain.

Figure 1.10 shows the fender of a fictional car[7]. The whole geometry consists of a bigger, uniformly curved part and a bulged-out, annular area that can be viewed as part of the wheel case. While it is possible to model the object by a single spline surface, it is much more convenient and natural to assemble it from two pieces. The ring-shaped part is modelled by an untrimmed standard spline surface **s**. The other part is an ABC-surface **a**, whose ribbon along the junction has C^1-contact with **s**, which is easy to achieve. This implies coinciding normals along the common boundary, and hence, by Theorem 2, a G^1 contact between **a** and **s**. The first plot shows the complete composite surface, while the second one features a zoom on a cross-section profile. The third and fourth plot show isophotes (which are continuos) and mean curvature (which is discontinuous), respectively.

---

[7] The geometry shown here was kindly provided by Malcolm Sabin, who modeled a similar composite G^2-surface using a completely different, hitherto unpublished technique.
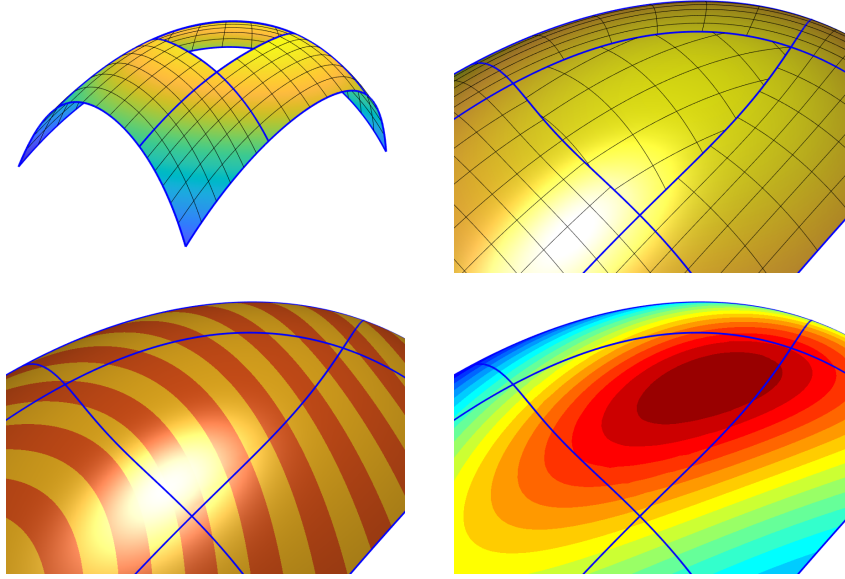
Fig. 1.11 Filling of a triangular hole – Arrangement of standard patches surrounding the hole *(top left)*, surrounding patches and ABC-filling with some parametric lines *(top right)*, isophotes *(bottom left)*, and mean curvature shading *(bottom right)*.

Figure 1.11 presents a classical hole-filling problem. Several standard spline surfaces are surrounding a triangular region, and another surface is sought that closes the gap smoothly. Here, we show that this can be achieved by an ABC-surface with three ribbons, each joining C^2 with the corresponding outer part. By Theorem 3, this guarantees a G^2-contact. The first plot shows the configuration defining the three-sided hole, and the second one the completed structure together with a few parameter lines. Isophotes and also the distribution of mean curvature, as shown by the third and fourth plot, indicate that the generated shape leaves little room for improvement.

1.6 Conclusion

All spline-based CAD systems currently in use are unable to generate composite spline surfaces that are watertight along trimming curves. We suggest ABC-surfaces as a solution to this problem. They are a special class of trimmed rational splines that match boundary information given in terms of so-called ribbons exactly, thus enabling the construction of G^k-continous joints. The framework is relatively sim-

ple and can be integrated seamlessly into existing CAD systems and file exchange formats. First experiments show that ABC-surfaces have good shape properties.

Future research will address the treatment of re-entrant corners and applications of the ABC-setup for the approximation of partial differential equations.

References

MH17.   B. Marussig and Th.J.R. Hughes. A review of trimming in isogeometric analysis: Challenges, data exchange and simulation aspects. *Archives of Computational Methods in Engineering*, 25:1–69, 2017.

MR.   B. Marussig and U. Reif. Surface patches with rounded corners. In preparation.

Pet02.   J. Peters. Geometric continuity. In M.S. Kim G. Farin, J. Hoschek, editor, *Handbook of Computer Aided Geometric Design*, pages 193–227. 2002.

PGVACN06.   N. Pla-Garcia, M. Vigo-Anglada, and J. Cotrina-Navau. N-sided patches with B-spline boundaries. *Computers and Graphics*, 30:959–970, 2006.

PR08.   J. Peters and U. Reif. *Subdivision surfaces*, volume 3 of *Series Geometry and Computing*. 2008.

Rei.   U. Reif. System and method for defining trimmed spline surfaces with accurate boundary control. Patent application EP19192703.7.

Rei97.   U. Reif. A refinable space of smooth spline surfaces of arbitrary topological genus. *Journal of Approximation Theory*, 90:174–199, 1997.

SVR14.   P. Salvi, T. Várady, and A.P. Rockwood. Ribbon-based transfinite surfaces. *Computer Aided Geometric Design*, 31(9):613 – 630, 2014.

VSK16.   T. Várady, P. Salvi, and G. Karikó. A multi-sided Bézier patch with a simple control structure. *Comput. Graph. Forum*, 35:307–317, 2016.

VSK17.   T. Várady, P. Salvi, and I. Kovács. Enhancement of a multi-sided Bézier surface representation. *Comput. Aided Geom. Des.*, 55:69–83, 2017.

VSR12.   T. Várady, P. Salvi, and A.P. Rockwood. Transfinite surface interpolation with interior control. *Graph. Model.*, 74:311–320, 2012.

VSVS20.   T. Várady, P. Salvi, M. Vaitkus, and A. Sipos. Multi-sided Bézier surfaces over curved, multi-connected domains. *Computer Aided Geometric Design*, 78:101828, 2020.

VVSS20.   M. Vaitkus, T. Várady, P. Salvi, and A. Sipos. Multi-sided B-spline surfaces over curved, multi-connected domains, 2020. Unpublished manuscript.